



Title	100KW Class Electron Beam Welding Technology (Report III) : Characteristics of Deep Penetration Bead and its Analysis
Author(s)	Arata, Yoshiaki; Tomie, Michio; Kohyama, Akira
Citation	Transactions of JWRI. 1976, 5(1), p. 11-18
Version Type	VoR
URL	<a href="https://doi.org/10.18910/8125">https://doi.org/10.18910/8125</a>
rights	
Note	

*The University of Osaka Institutional Knowledge Archive : OUKA*

<https://ir.library.osaka-u.ac.jp/>

The University of Osaka

# 100KW Class Electron Beam Welding Technology (Report III) † —Characteristics of Deep Penetration Bead and its Analysis—

Yoshiaki ARATA\*, Michio TOMIE\*\* and Akira KOHYAMA\*\*\*

## Abstract

The welding of thick plates was carried out by the 100 KW class electron beam welder as shown in Ref.(1). As a result, the characteristics of deep penetration welding could be studied, in relation to the application of high power electron beam to several kinds of thick steel plates.

Furthermore, investigation was made into welding defects peculiar to the welding electron beam and the structure of weld metal.

## 1. Introduction

For the one pass welding of steel plates over 100 mm thickness with a short time, only the electron beam energy with very high levels of the power and its density is available.<sup>1),3),4)</sup> Using such electron beam welding, in the case of small bead width, this welding will have quick heating and cooling rate. In this instance, however, welding defects, which appear concurrently with solidification as peculiar to the electron beam welding, are often observed dangerously.

Concerning the weldability of the above, several reports are available about a case of a few centimeters penetration at a low power, but no detailed report is made public about a case of a high power of 50 KW and upwards. Under the circumstances, study was made about the weldability of mild and high tensile steel plates as using a high power electron beam welder,<sup>1)</sup> which plates were extensively used for large structures.

## 2. Materials and welding conditions

The test specimens used were taken from steel plate (SS41) for general structure, steel plate (SM41) for welding structure and high tensile steel plates (HT 60 and HT80) for welding structure, all available in the market. Their chemical composition is shown in Table 1. The electron beam power of the welder is 50KW and 100KW ( $V_b = 100$  KV constant).

Table 1. Chemical composition of material used.

	Wt(%)											PPm	
	C	Si	Mn	P	S	Cu	Cr	Ni	Mo	V	B	O	N
HT80	0.11	0.32	0.92	0.008	0.006	0.26	0.46	1.03	0.47	0.03	0.0012	10	34
HT60	0.14	0.30	0.88	0.008	0.008	—	0.26	0.45	0.23	0.05	—	20	33
SM41	0.18	0.47	0.71	0.015	0.010	—	—	—	—	—	—	36	68
SUS304	0.05	0.74	1.74	0.030	0.010	0.12	1.95	10.9	0.16	—	—	75	360
SS-41 KILLED	0.21	0.29	1.25	0.016	0.011	—	—	—	—	0.08	—	20	36
SS-41 SEM KILLED	0.18	0.03	0.87	0.009	0.015	0.23	0.26	—	—	—	—	230	42

By use of the AB-test method,<sup>2)</sup> the electron beam was preliminarily checked in respect of its form, and the focus ( $D_F$ ) of the beam as applied for welding was taken at 500 mm. Also, the active beam parameter ( $\alpha_b$ ) was fixed at 0.9 of a value which ensures a maximum penetration depth. The beam was deflected at a set-back angle of 10 degrees, in order to restrain the arcing of the electron beam gun due to metal vapour as generated during welding.

## 3. Test results and observation

Fig. 1 shows an effect of welding speed ( $v_b$ ) upon penetration depth ( $h_p$ ) at 50 KW and 100 KW beam outputs, and it is seen from this Fig. 1 that relations of  $h_p \propto 1/\sqrt{v_b}$  are approximately established for both beam outputs at welding speed over a certain level. In the case

† Received on Jan. 19, 1976

\* Professor

\*\* Research Associate

\*\*\* Dept. of Metallurgy and Materials Science, Faculty of Engineering, Tokyo University

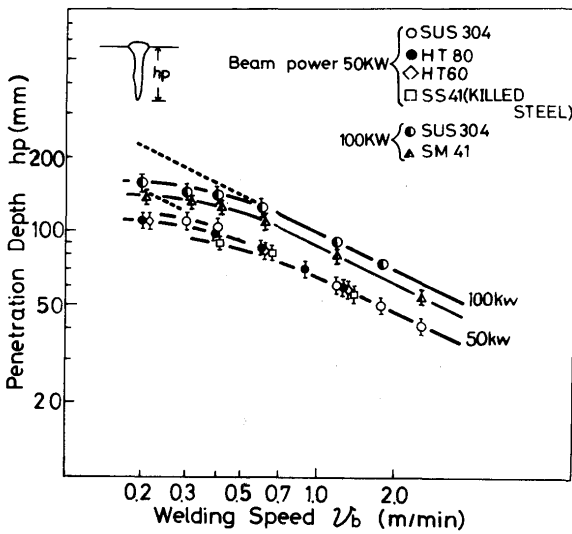


Fig. 1 Relations between  $v_b$  and  $h_p$

of 50 KW beam output,  $h_p \propto 1/\sqrt{v_b}$  can be observed, when the welding speed is higher than 50 cm/min. The penetration depth ( $h_p$ ), however, begins to be saturated, when the speed is lower than 50 cm/min. This saturation is caused, because molten metal once flowed back in a beam hole formed by deep penetration, is re-heated by the beam and energy necessary for the deep penetration is lost. Photo. 1 shows the longitudinal cross sections of the flat position welding bead on the steel plates (HT80

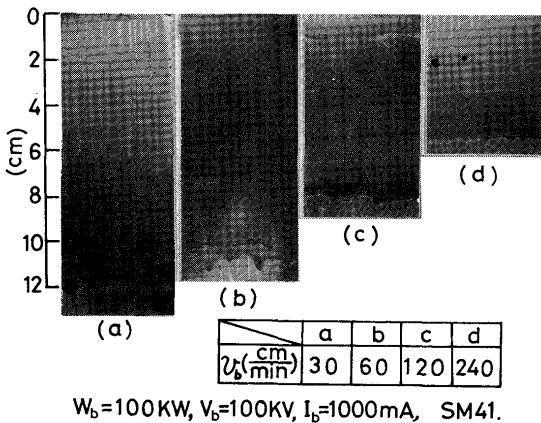
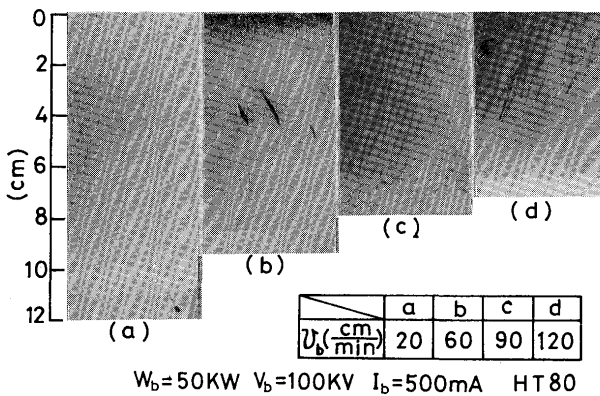


Photo. 1 Longitudinal cross sectional view of the bead for HT80 and SM41

and SM41). The penetration is well form and it is observed that the bead appearance deteriorates with a drop in welding speed. As welding defects, A-porosity (active zone porosity) and R-porosity<sup>5)</sup> are generally observed. The former frequently occurs around the center of the penetration depth and more along the ripple line on the longitudinal cross section at the bead center line, and the latter is much observed to be surrounded by the dendrite at the vicinity of the bottom or spiking of the bead.

As welding defects liable to be caused by use of high power electron beam, there are (1) blowhole, (2) A-porosity, (3) R-porosity, (4) cold shut and cold shut crack and (5) horizontal crack.

(1) Blowhole

The occurrence of blowholes can be avoided, if a parent material contains a minimum amount of gases, and they do not appear in high tensile and killed steel plates.

Photo. 2 shows a case of blowholes in semi-killed steel. It is seen that beads are abruptly disordered due to

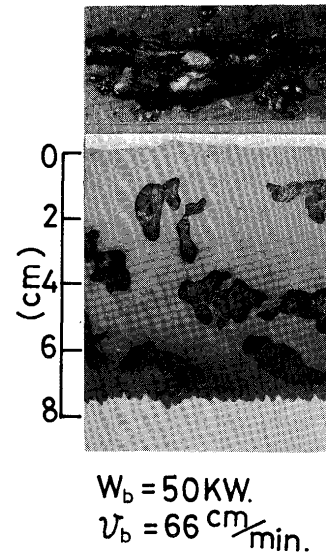
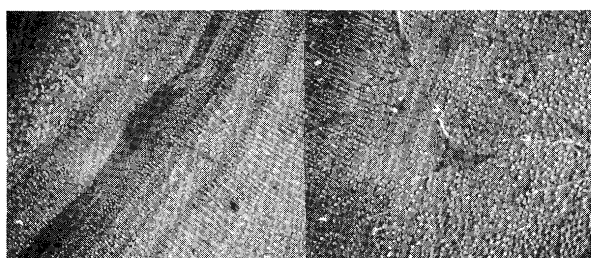


Photo. 2 Bead appearance and longitudinal cross section for Semi-killed steel.

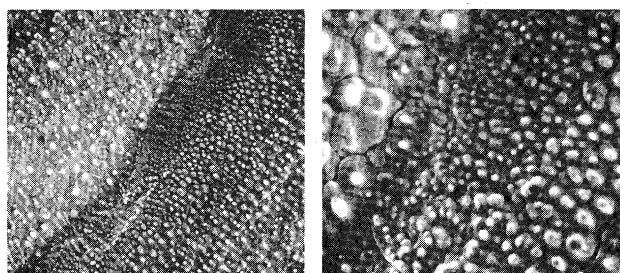
the blowing of gases from the parent material. Photo. 3 shows scanning electron micrographs of defective surfaces. The many solidification tip parts of the dendrites can be observed. It is to be noted that gaseous contents of about 50 ppm does not matter in the formation of blowholes, but when the contents are about 100 ppm, the occurrence of blowholes depends upon a welding condition, which behavior is very complicated.

(2) A-Porosity

This porosity is frequently observed especially in the penetration of wine bottle form, but appears with a slight



(x100x $\frac{1}{2}$ )

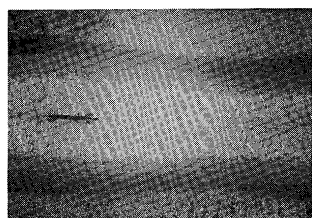


(x300x $\frac{1}{2}$ )

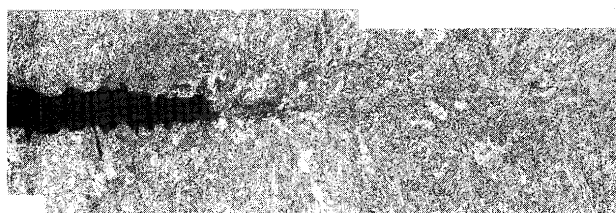
(x1000x $\frac{1}{2}$ )

Photo. 3 Scanning electron micrographs of porosity surface ( $W_b = 50 \text{ KW}$ ,  $v_b = 60 \text{ cm/min}$ , Semi-killed steel)

change in bead width, even in the case of the “well-form” penetration. In most cases, A-Porosity occurs in the weld metal containing alloy elements of high vapor pressure



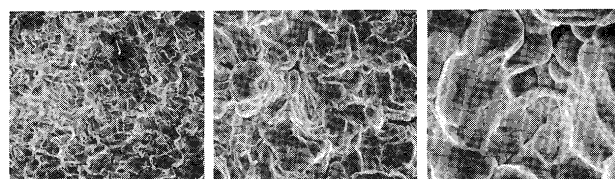
Welding direction  $\rightarrow$  (x7x $\frac{1}{2}$ )



(x100x $\frac{1}{2}$ )

Photo. 4 Horizontal cross section of HT80 weld metal ( $W_b = 50 \text{ KW}$ ,  $v_b = 60 \text{ cm/min}$ )

and over than certain level of amount of gases. Photo. 4 shows a horizontal cross section of weld metal and the occurrence of A-porosity. In this case, it has a nugget structure and is accompanied with free dendrite formed around its edge in an anti-welding direction, though the occurrence of another type is recognized.<sup>5)</sup> For the mechanism of A-porosity occurrence, It depends on the kinds of parent material and welding conditions. Photo. 5

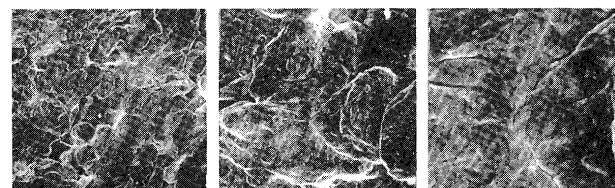


(x100x $\frac{1}{2}$ )

(x300x $\frac{1}{2}$ )

(x1000x $\frac{1}{2}$ )

Photo. 5 Scanning electron micrographs of porosity surface ( $W_b = 50 \text{ KW}$ ,  $v_b = 40 \text{ cm/min}$ , HT80)



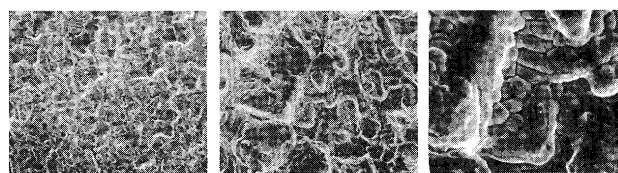
(x100x $\frac{1}{2}$ )

(x300x $\frac{1}{2}$ )

(x1000x $\frac{1}{2}$ )

Photo. 6 Scanning electron micrographs of porosity surface ( $W_b = 50 \text{ KW}$ ,  $v_b = 20 \text{ cm/min}$ , HT60)

and 6 show scanning electron micrographs of the A-porosity surface of high tensile steel. From both of these Photograph, it can be inferred that the defect is formed by a condition similar to shrinkage cavity in casting. Namely, Photo. 5 relates to the central part of the A-porosity and a solidified structure develops at right angles with the steel surface. It is observed that the structure has underwent a slight deformation just before solidification. On the other hand, the A-porosity in Photo. 6 is found in the vicinity of a weld end and the solidified structure, undergoes a substantial deformation. In this respect, the formation of the porosity is attributable to a cause different from the case of a blowhole as formed due to a heavy



(x100x $\frac{1}{2}$ )

(x300x $\frac{1}{2}$ )

(x1000x $\frac{1}{2}$ )

Photo. 7 Scanning electron micrographs of porosity surface ( $W_b = 50 \text{ KW}$ ,  $v_b = 40 \text{ cm/min}$ , Killed steel)

existence of gases. Photo. 7 shows a case of mild steel (killed steel) and a phenomenon similar to the case of high tensile steel can be observed. Furthermore, a similar phenomenon can be observed in the case of 100 KW output.

### (3) R-porosity

As in the case of A-porosity, R-porosity is frequently surrounded with dendrite extended toward a welding direction, and it is formed when the molten fluid un-fills

space which is produced by boiling in the bottom weld metal. Photo. 8 shows scanning electron micrographs of the R-porosity surface, and it is seen that this is a quickly

steel and others of high sulfur content. This crack is considered to be hot cracking due to a deformation at the time of solidification. Also, some small horizontal cracks are considered to be attributable to the insufficient fluidity and amount of molten metal, similar to the case of the A-porosity.

The most basic cause for the occurrence of such defects should generally be found in the stability of a beam hole formed by electron beam. In relation to this fact, weld position should be taken into consideration. In the case of flat position welding by the application of vertical beam, full penetration of good structure can be expected, and more full penetration of better structure is obtained by horizontal beam compared with vertical beam. Especially<sup>6)</sup>, the beam hole can be maintained at the most stable condition, in the case of upward vertical position welding by the horizontal beam. It seems that the most effective improvements for the welding defects can be expected in that instance.

Another problem in the deep penetration by the electron beam welding is related to the strength of the welded part. That is, it is concerned with the uniformity of structure in a direction of plate thickness. We have no exact data about this problem as yet.

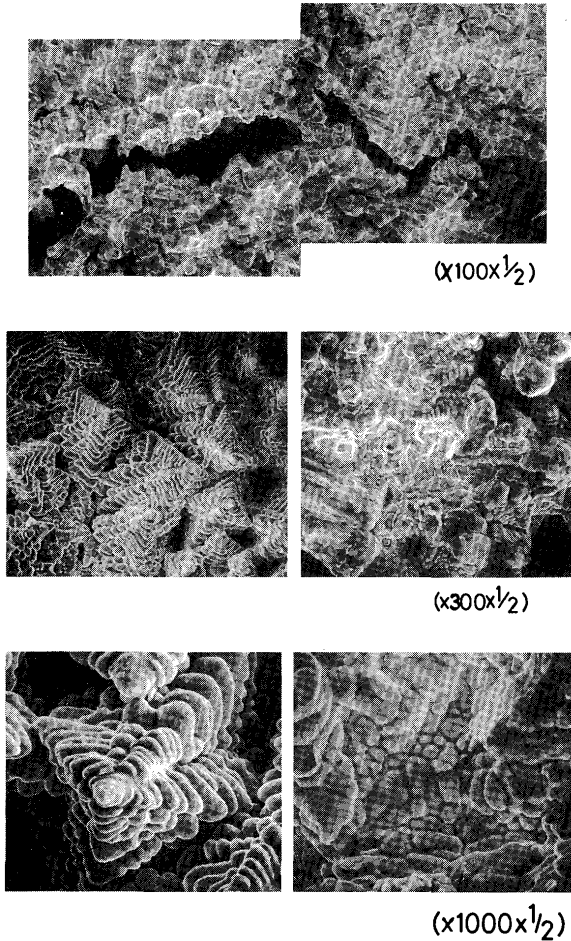


Photo. 8 Scanning electron micrographs of porosity surface ( $W_b= 50 \text{ KW}$ ,  $v_b= 40 \text{ cm/min}$ , Killed steel)

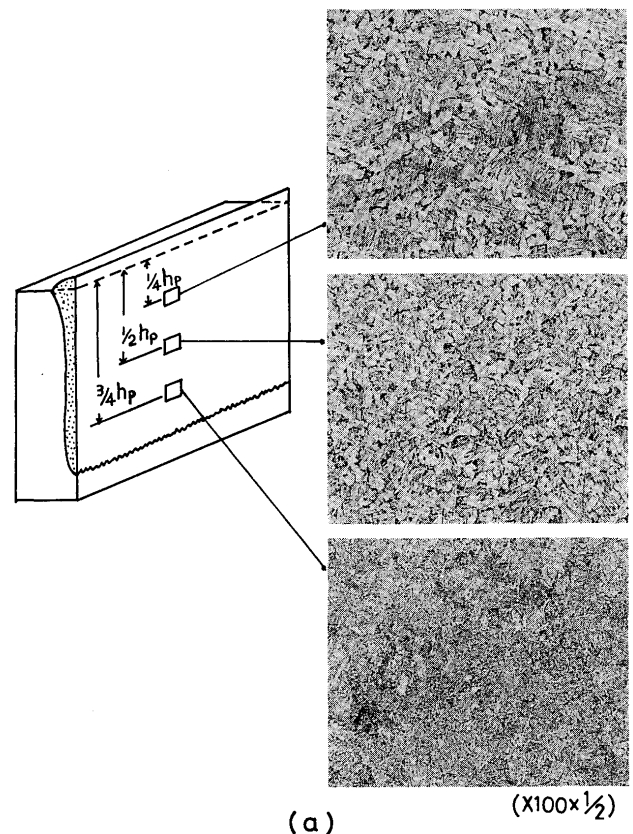
cooled solidified structure. In Photo. 8, a crack is shown at right angles with the photograph which is enlarged up to 100 times and this is a horizontal crack.

(4) Cold shut and cold shut crack

The formation of a large spike frequently leaves room where the cold shut and its crack which are liable to be caused along the ripple line in the bottom side, and it is not so easy to eliminate completely the cold shut and its crack. Especially when deep penetration weld is applied and the reheating phenomenon of the molten pool is occurring, spike become large and both of cold shut and cold shut crack are liable to take place.

(5) Horizontal crack

As shown in Photo. 1 and 2, in most cases, a horizontal crack occurs concurrently with the A-porosity and the R-porosity. Its occurrence is frequently observed in mild



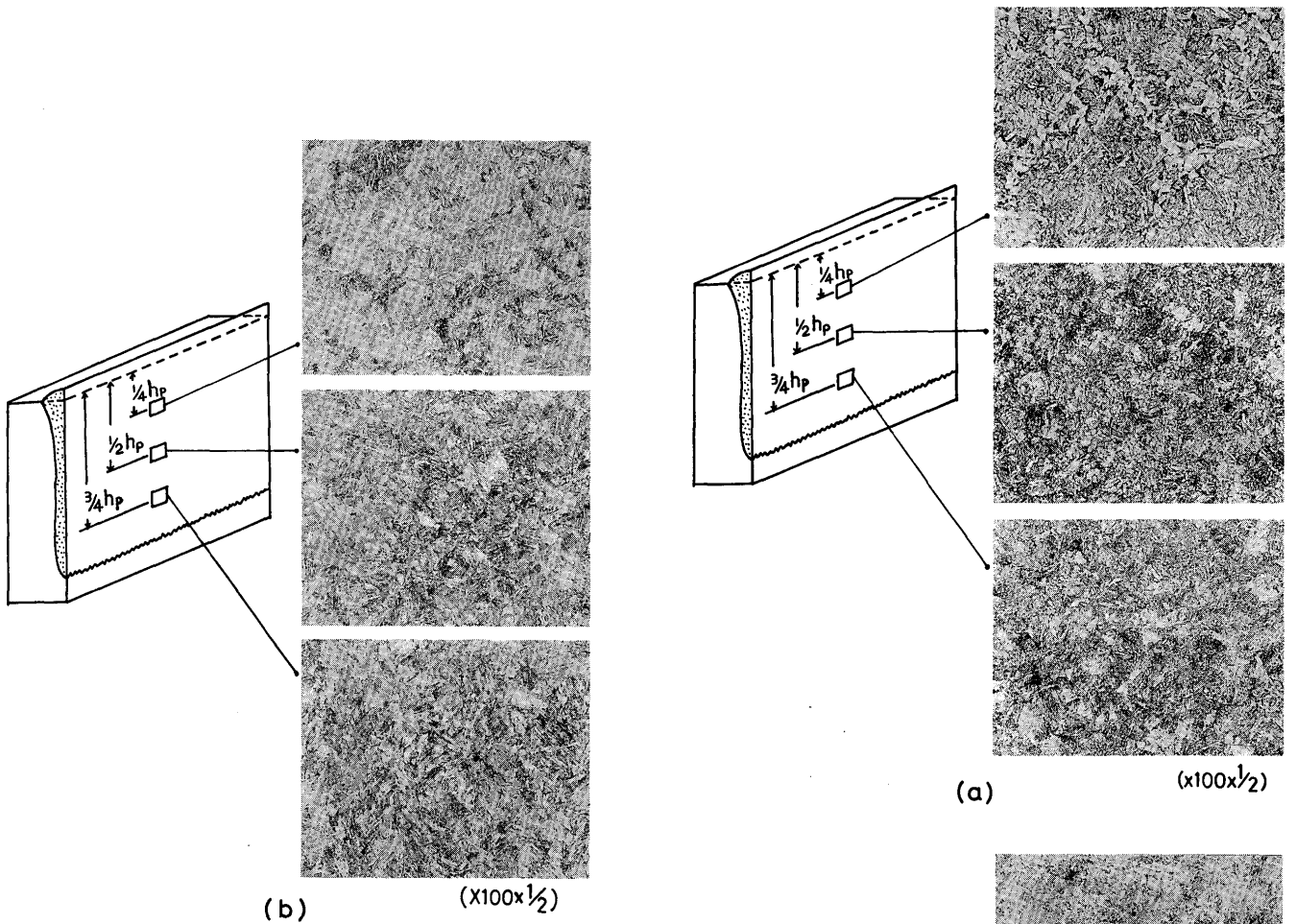


Photo. 9 Microstructure of HT80 weld metal.  
 ( $W_b = 50KW$ , (a);  $v_b = 20$  cm/min, (b);  $v_b = 120$  cm/min)

Photo. 9(a) and (b) show the microstructure of HT80 weld metal, and a difference of structure at  $\frac{1}{4}$  depth,  $\frac{1}{2}$  depth and  $\frac{3}{4}$  depth from the surface is shown for two welding speeds of 20 cm/min and 120 cm/min. In the case of (a), ferrite structure with large ferrite as initially noticed is found at  $\frac{1}{4}$  depth and the initial ferrite becomes small at  $\frac{1}{2}$  depth, gradually changing into micro ferrite structure. On the other hand, bainite is formed at  $\frac{3}{4}$  depth and it is inferred that a substantial difference of toughness as well as strength is existing at that portion.

Photo. 10(a) and (b) are related to HT60 weld metal and it is seen that the structure gives a broad difference, depending upon the position of beads (direction of penetration), similar to the case of HT80 weld metal.

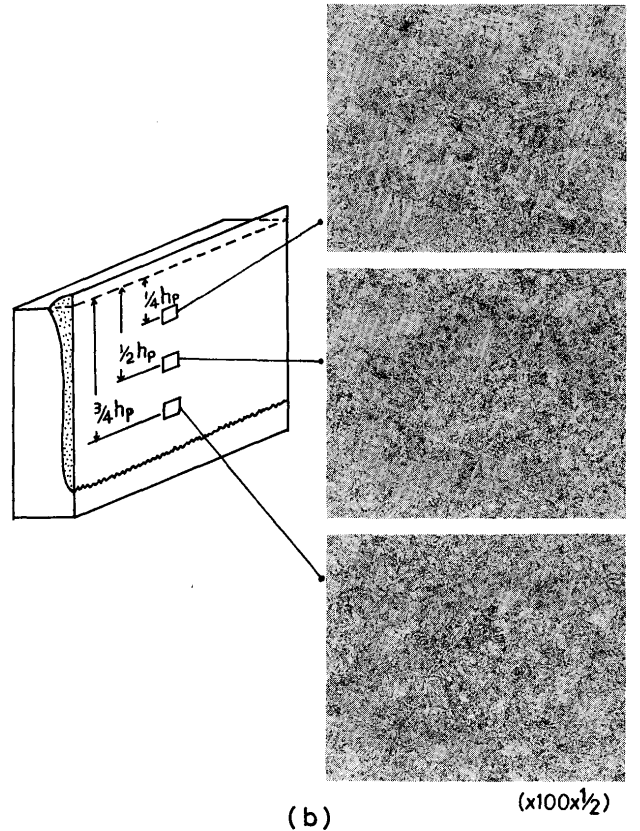


Photo. 10. Microstructure of HT60 weld metal  
 ( $W_b = 50KW$ , (a);  $v_b = 20$  cm/min, (b);  $v_b = 120$  cm/min)

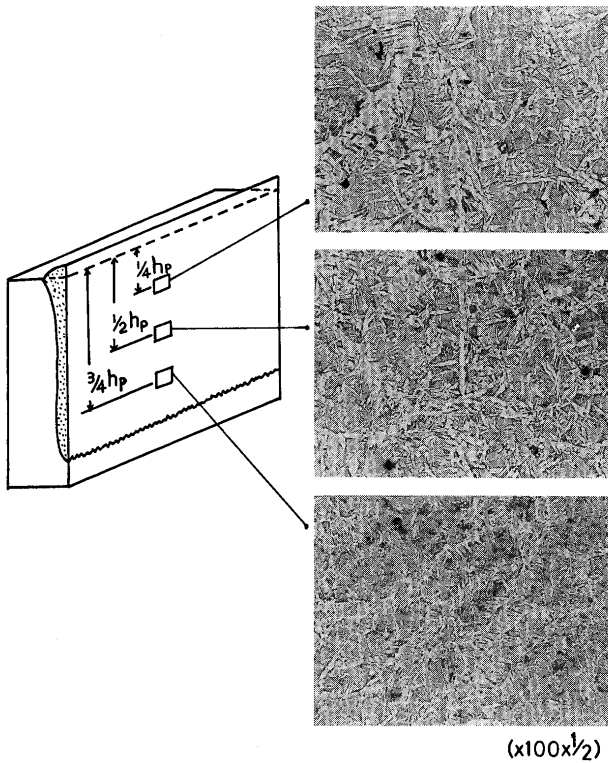


Photo. 11. Microstructure of SM41 weld metal ( $W_b = 100KW$ ,  $v_b = 20$  cm/min)

Photo. 11 shows a case of SM41 weld metal obtained by 100KW electron beam welding. The hardness distribution of the welded part of HT80 is shown in Fig. 2 which indicated that maximum hardness changes conspicuously,

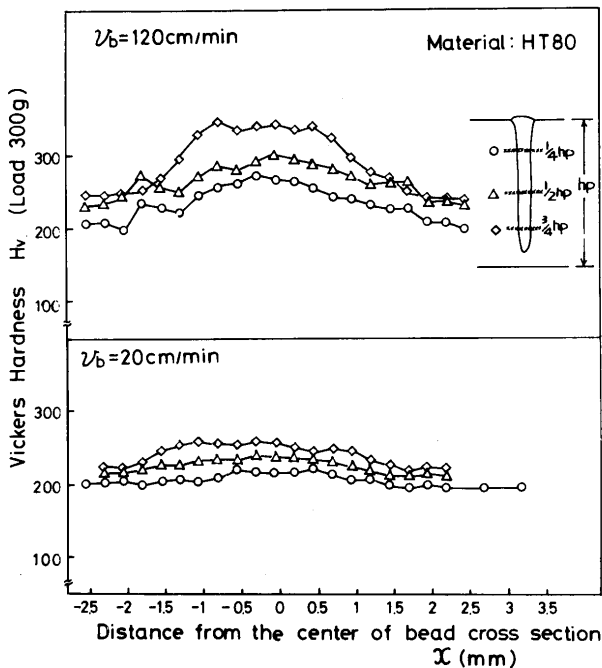


Fig. 2. Hardness curves for welded part of HT80 ( $W_b = 50KW$ )

depending upon a position on the cross sectional bead. Also, it is not observed that a very high maximum hardness is usually recognized at the bonded part around 20~30 mm depth from a steel surface. Fig. 3 shows a case of

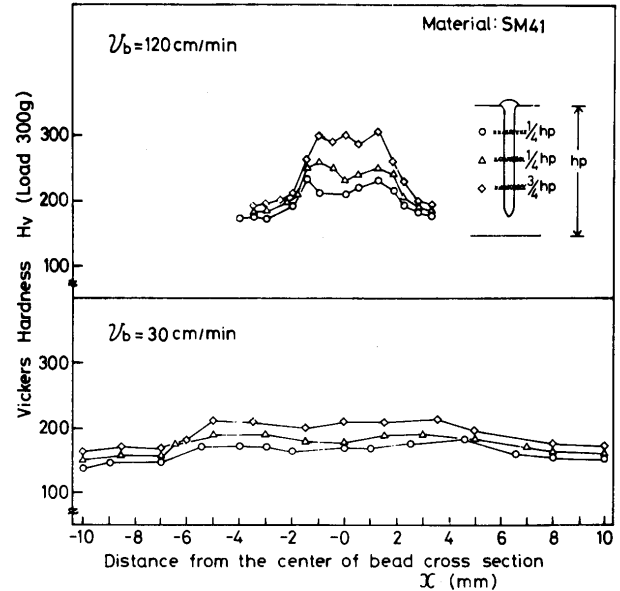


Fig. 3. Hardness curves for welded part of SM41 ( $W_b = 100KW$ )

SM41 weld metal. Now, the chemical compositions of HT60 and HT80 weld metals are shown in Table 2. It is seen that only manganese drops in amount and sulfur and

Table. 2 Chemical composition of weld metal.

Mark	$X^*$	C	Si	Mn	P	S	Cu	Cr	Ni	Mo	V	B
HT 80	1/4 hp	0.11	0.30	0.70	0.008	0.006	0.24	0.46	1.03	0.47	0.03	0.0012
	1/2 hp	0.10	0.29	0.76	"	"	"	"	"	"	"	"
	3/4 hp	0.11	"	0.81	"	"	0.25	"	"	"	"	"
HT 60	1/4 hp	0.14	0.30	0.71	"	0.008	—	0.24	0.45	0.23	0.05	—
	1/2 hp	0.13	"	0.74	"	"	—	"	"	"	"	—
	3/4 hp	"	"	0.80	"	"	—	"	"	"	"	—

$X^*$ : Distance from specimen surface  
 WELDING CONDITION Beam Power 50KW(100KV,500mA)  
 Welding speed 20cm/min

phosphorus having a high vapor pressure, undergo little change, due to their small absolute amount. In order to make uniform the chemical composition of weld metal, it would be recommended to add an alloy element to the specimen surface and cause a density grade in a direction of plate thickness. For this purpose, the electron beam is impinged upon the usual welding electrode of 2¼Cr-1Mo steel which is placed on the specimen surface, as shown in Fig. 4. In the case of 50 KW beam output and 120 cm/min welding speed, chrome density changes so that it is 0.59% at 1/4 depth from the surface and 0.50% at 3/4 depth from the surface respectively, as shown in Table 3. Also, the structure of weld metal is identical at 1/2 and 3/4

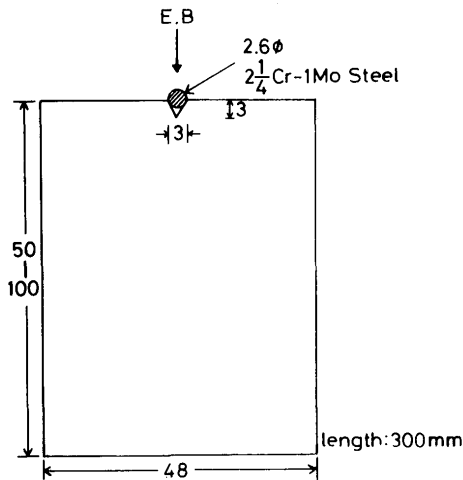


Fig. 4. Specimen preparation for Cr-Mo addition from specimen surface, using usual welding electrode of 2 1/4 Cr-1Mo steel.

Table. 3 Chemical composition of weld metal.  
(Cr-Mo Addition from specimen surface)

$\chi^*$	C	Si	Mn	P	S	Cu	Cr	Ni	Mo	V	B
1/4 hp	0.08	0.33	0.82	0.007	0.007	0.24	0.59	0.98	0.51	0.02	0.0012
1/2 hp	"	"	0.83	"	"	"	0.55	"	0.50	"	"
3/4 hp	0.10	"	0.87	"	"	"	0.50	1.00	"	"	"
M.M.**	0.11	0.32	0.92	0.008	0.006	0.26	0.46	1.03	0.47	0.03	0.0012

(\*) Distance from specimen surface  
 (\*\*\*) Mother Material  
 Welding Condition: Beam power 50KW(100KV, 500mA)  
 Welding speed 120 cm/min  
 insert metal 2 1/4 Cr-1Mo steel  
 Welding rod (2.6 $\phi$ )

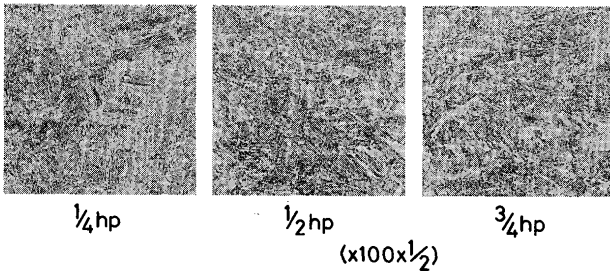


Photo 12 Microstructure of HT80 weld metal.  
(Cr-Mo addition from specimen surface  
 $W_b$ : 50KW,  $u_b$ : 120 cm/min)

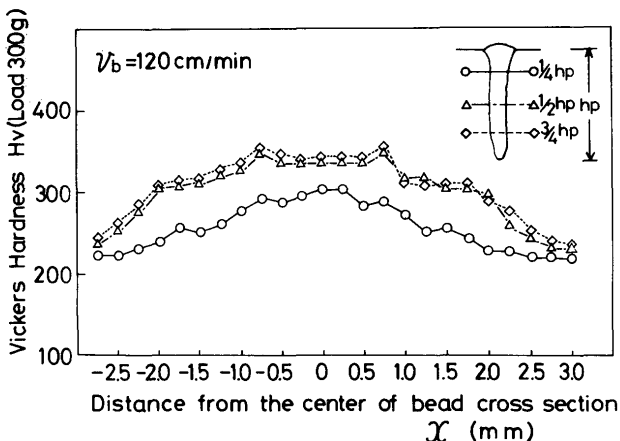


Fig. 5 Hardness curves for welded part of HT80, ( $W_b$ =50KW)

from its surface, as shown in Photo. 12. Fig. 5 shows a hardness distribution at the welded part. It is observed that there is no difference of hardness at 1/2 and 3/4 depth from the surface, and a difference between the maximum hardness and hardness at 1/4 depth is only less than 50 by  $H_p$ -values. Thus, it is concluded that the addition of chrome to the specimen surface is effective to unify about each chemical composition and the structure of weld metal.

4. Conclusion

Study was made about the problems of the deep penetration welding of thick steel plates using the high power electron beam welding method, and the following conclusions were obtained.

- (1) Stainless, mild and high tensile steel plates were welded and in the case of the stainless steel (SUS 304), the maximum penetration depth from the surface was 120 mm at a 50 KW beam power and 160 mm at a 100 KW beam power respectively. In the case of high tensile steel, it was 110 mm and 140 mm respectively.
- (2) With beam powers of 50 KW and 100 KW,  $h_p \propto 1/\sqrt{u_b}$  can be observed, if the welding speed is over 50 cm/min. The penetration depth  $h_p$  is approximately constant, if the welding speed is lower than 20 cm/min. In a region of welding speed under 50 cm/min, a phenomenon of reheating molten metal by electron beam is taking place due to the violent "wall-fluctuation" of the beam hole.
- (3) Welding defects as observed were a blowhole, A-porosity, R-porosity, a cold shut, cold shut crack and a horizontal crack. For these defects, its surfaces were carefully observed by the help of scanning electron micrographs, to find out a cause for the occurrence of the defects. As a result, it was concluded that the upward vertical position welding by horizontal beam should be adopted and its full penetration weld should be recommended, in order to avoid the occurrence of these welding defects for the thick plates.
- (4) In the large power electron beam welding, the bonded part is free from abnormal hardening, but the structure of the welded part gives a substantial change in a direction of plate thickness. It is also clarified that the mechanical properties of the welded part are seriously affected by such structure. This problem needs special attention in a region where a phenomenon of re-heating molten metal by electron beam appears.
- (5) In order to minimize the structural change of the welded part in the penetrated direction, investigation was made into the addition of an alloy element

(chrome in this report) to the specimen surface. As a result, it was found possible to unify the structure of the welded part in the penetrated direction.

#### Acknowledgement

The authors would like to express their gratitude to Dr. K. Ito, Prof. Dr. N. Igata and Dr. N. Oda for their encouragements.

#### References

- 1) Y. Arata, M. Tomie: "100 KW Class Electron Beam Welding Technology (Report I)", Trans. of JWRI, vol. 2, No. 1 (1973); "100 KW Klasse-Elektronenstrahlen-Schweißtechnologie (Bericht II)", Trans. of JWRI, vol. 4, No. 1 (1975)
- 2) Y. Arata, M. Tomie, K. Terai, H. Nagai and T. Hattori: "Shape Decision of High Energy Density Beam" Trans. of JWRI, vol. 2, No. 2 (1973)
- 3) A. Sanderson; A 75KW Electron Beam Installation for Thick Section Welding, Proc. Conf. on Advances in Welding Processes, Harrogate (1974) The Welding Institute.
- 4) G. Sayegh, P. Dumonte and T. Nakamura Design and Manufacture of a 100 KW Electron Gun, Advanced Welding Technology. The Second International Symposium of J.W.S., August (1975)
- 5) Y. Arata, K. Terai and S. Matsuda: Study on Characteristics of Weld Defect and Its Prevention in Electron Beam Welding (Report I)—Characteristics of Weld Porosities—, Trans. of JWRI, vol. 2, No.1 (1973)
- 6) Y. Arata, M. Osumi, K. Higuchi and K. Noda: Study on Electron Beam Welding of High Strength Aluminum Alloy, Preprints of the National Meeting of J.W.S. No.16 (Spring 1975) (In Japanese).; Advanced Welding Tech., The Second Int. Symp. August (1975)